PAPER

The nanoscale structure and unoccupied valence electronic states in FeSe$_{1-x}$Te$_x$ chalcogenides probed by X-ray absorption measurements†

M. Y. Hacisalihoglu,[abc] E. Paris,[ad] B. Joseph,[ae] E. Yanmaz[c] and N. L. Saini*[a]

We have studied the nanoscale structure and unoccupied electronic states in FeSe$_{1-x}$Te$_x$ by a combined analysis of Se K, Te L$_1$ and Fe K-edges X-ray absorption measurements. Extended X-ray absorption fine structure (EXAFS) results show that iron–chalcogen (Fe–Se and Fe–Te) distances in ternary FeSe$_{1-x}$Te$_x$ are similar to those measured for binary FeSe and FeTe. The local Fe–Se/Te distances determined by different absorption edges fit well in the characteristic Z-plot of random alloys, providing unambiguous support to the inhomogeneous nanoscale structure of the ternary FeSe$_{1-x}$Te$_x$ system. X-ray absorption near-edge structure (XANES) spectra reveal a gradual evolution of the unoccupied valence electronic states as a function of Te-substitution in FeSe$_{1-x}$Te$_x$. The Fe 3d–Se 4p/Te 5p hybridization is found to decrease with Te-substitution, accompanied by an increase in unoccupied Se 4p states and a decrease in unoccupied Te 5p states. The results are discussed in the frame of local inhomogeneity in the FeSe$_{1-x}$Te$_x$ system driven by random alloying of Se/Te atoms.

1 Introduction

The discovery of superconductivity in the layered binary FeSe with $T_c \sim 8$ K[1] has been pivotal in the field of iron-based superconductors, stimulating several studies. This was due to the fact that basic electronic structure of this binary system is similar to the other iron-based superconductors,[2,3] driven by Fe 3d states, while the crystal unit cell is much simpler,[4–6] containing just FeSe$_4$-tetrahedra stacked along the c-axis without any spacer layers. Shortly after the discovery it was found that T_c of FeSe can be raised up to ~ 15 K in FeSe$_{1-x}$Te$_x$ by chemical substitution,[7,8] and up to ~ 37 K by external pressure.[9,10] It was also made clear that the defect chemistry plays an important role in the transport properties of this 11-family of superconducting chalcogenides. Soon, it was clear that the FeSe$_{1-x}$Te$_x$ system contains nanoscale inhomogeneities.[11] Indeed, experimental probes sensitive to the local structure, *e.g.* pair distribution function (PDF) analysis of X-ray and neutron diffraction[12] and

extended X-ray absorption fine structure (EXAFS) analysis,[11,13–15] have clearly shown that the ternary FeSe$_{1-x}$Te$_x$ system is characterized by distinct Fe–Se and Fe–Te bond lengths as in the random alloys.[16] Furthermore, scanning transmission electron microscopy (STEM)[17] and scanning tunneling microscopy (STM)[18–21] have also shown nanoscale electronic inhomogeneities in FeSe$_{1-x}$Te$_x$.

Iron-based superconductors are multiband systems[2,3] and a small inhomogeneity or a disorder can have a substantial effect on the electronic properties of such systems. Therefore, the knowledge of the local atomic structure and the unoccupied electronic density of states as a function of substitution in FeSe$_{1-x}$Te$_x$ should be an important criterion for finding possible correlations between the local structure and the electronic properties. EXAFS is an atomic-site selective method, providing information on the local atomic distribution around a selected absorbing atom through scattering of the photoelectrons excited from the X-ray absorbing atom with the nearest neighbours.[22] On the other hand, X-ray absorption near edge structure (XANES) spectroscopy is a valuable finger print local probe of unoccupied valence states and higher order atomic correlations. Here, we have used EXAFS and XANES measurements at Se K, Te L$_1$ and Fe K-edges to probe the local structure and the electronic structure of unoccupied valence states in FeSe$_{1-x}$Te$_x$ for different Te-concentrations. We have exploited the atomic site selective sensitivity of EXAFS to separately resolve the local nanoscale environment surrounding the absorbing atoms, with aim of obtaining complete information on the local structure of the system.

a Dipartimento di Fisica, Università di Roma "La Sapienza", P. le Aldo Moro 2, 00185 Rome, Italy. E-mail: Naurang.saini@roma1.infn.it; Fax: +39 06 49694323; Tel: +39 064991 4387

b Department of Physics, Recep Tayyip Erdogan University, 53100 Rize, Turkey

c Department of Physics, Karadeniz Technical University, 61080 Trabzon, Turkey

d Center for Life NanoScience@Sapienza, Istituto Italiano di Tecnologia, V. le Regina Elena 291, 00185 Rome, Italy

e Elettra, Sincrotrone Trieste, Strada Statale 14, Km 163.5, Basovizza, Trieste, Italy

† Electronic supplementary information (ESI) available. See DOI: 10.1039/c5cp01740h

This journal is © the Owner Societies 2015

Phys. Chem. Chem. Phys., 2015, **17**, 18131–18137 | **18131**

It is found that, consistent with earlier studies on the local structure, ternary $FeSe_{1-x}Te_x$ contains nanoscale inhomogeneities characterized by coexisting Fe–Se and Fe–Te bondlengths. The Fe K-edge XANES spectra show that Fe 3d–Se 4p/Te 5p hybridization tends to decrease with increasing Te-content. The Se K-edge (Te L_1-edge) XANES spectra reveal that the unoccupied Se 4p (Te 5p) states increase (decrease) with the Te-substitution. These particular characteristics of $FeSe_{1-x}Te_x$ should have direct implications for the functional properties of $FeSe_{1-x}Te_x$, and the results should serve as important feedback for the theoretical models to describe properties of the iron-based superconductors.

2 Experimental methods

Single-crystalline samples of $FeSe_{1-x}Te_x$ were prepared using a temperature gradient method.[23] High purity Fe pieces (99.9+%), Se shots (99.99%) and Te lumps (99.997%) were used as precursor materials, mixed in stoichiometric ratios and kept in an alumina crucible that was sealed in quartz tubes under vacuum of 10^{-5} mbar. The quartz tubes were inserted into a two zone horizontal furnace, heated slowly up to ~ 650 °C, and kept at this temperature for 12 h. This was followed by a simultaneous heating of the two zones up to ~ 970 °C and ~ 950 °C chosen from binary phase diagrams.[24,25] The temperature was held for 24 h. Thereafter cold and hot zones of the furnace cooled down to 450 °C at a rate of 5 °C h^{-1} and finally the furnace was turned off to cool down to room temperature. The samples were characterized for their crystal structure using X-ray diffraction measurements performed using a Huber G670 Guinier imaging plate diffractometer (Co-K$_{\alpha 1}$ X-rays generated at 40 kV and 30 mA). The powder X-ray diffraction patterns (e.g., Fig. S1 shown as ESI†) were indexed using a tetragonal $P4/nmm$ space group, showing small amounts of impurities of the hexagonal Fe_7Se_8 phase and unreacted iron in binary FeSe, however, ternary $FeSe_{1-x}Te_x$ were found to be free from any detectable impurity phase. The transport properties, including the superconductivity, are reported elsewhere.[23]

Se K-edge, Te L_1-edge and Fe K-edge X-ray absorption measurements were performed at the XAFS beamline of the Elettra synchrotron radiation facility, Trieste, where the synchrotron radiation emitted by a bending magnet source was monochromatized using a double crystal Si(111) monochromator. Finely powdered samples of $FeSe_{1-x}Te_x$ were mixed uniformly in an organic matrix and pressed into pellets of 13 mm diameter for obtaining the edge jumps to be about 1. The measurements were made at room temperature in the transmission mode using three ionization chambers mounted in a series for simultaneous measurements on the sample and a reference. Several X-ray absorption scans were collected to ensure the reproducibility of the spectra and a high signal to noise ratio. The EXAFS oscillations were extracted by the standard procedure based on the cubic spline fit to the pre-edge subtracted absorption spectrum.[22] On the other hand, the XANES spectra were

normalized with respect to the atomic absorption estimated by a linear fit far away from the absorption edge jump.

3 Results and discussion

Here, we start with the presentation of the local structure results obtained by EXAFS. Fig. 1 shows Fourier transforms (FTs) of the EXAFS oscillations extracted from Se K-edge (upper), Te L_1-edge (middle) and Fe K-edge (lower) X-ray absorption spectra measured on $FeSe_{1-x}Te_x$ samples. The FTs are performed using the Gaussian windows with the k ranges being 3–17 Å^{-1}, 3–14 Å^{-1} and 3–16 Å^{-1}, respectively, for the Se K-edge, Te L_1-edge and Fe K-edge EXAFS. These FTs provide information on the atomic distributions around the photo-absorbing Se, Te
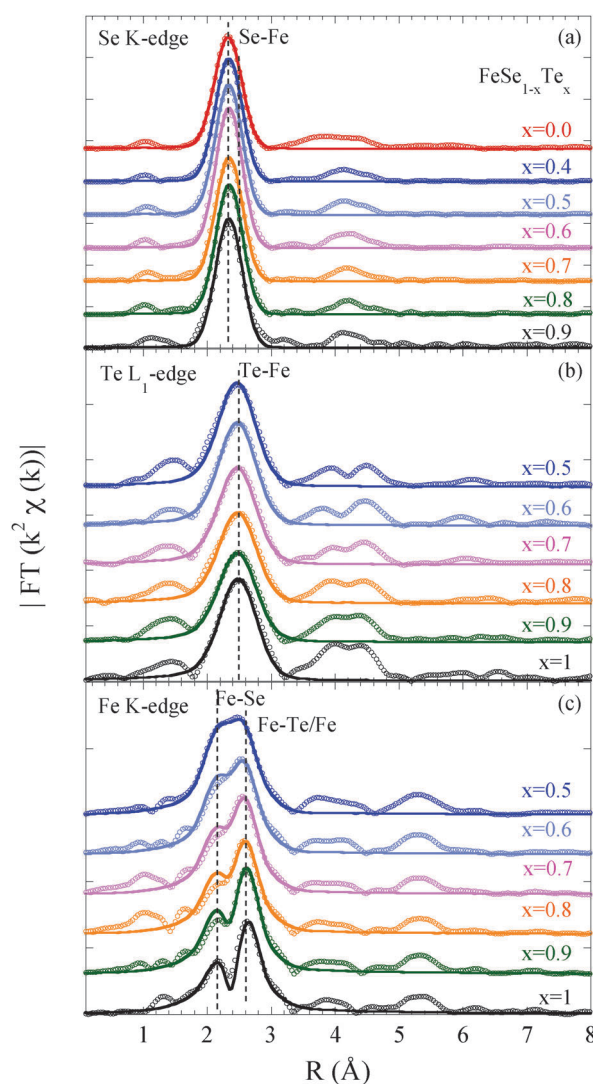

Fig. 1 Fourier transform (FT) magnitudes of the k^2-multiplied EXAFS oscillations at Se K-edge (upper), Te L_1-edge (middle) and Fe K-edge (lower) measured on $FeSe_{1-x}Te_x$ for several Te-concentrations. The FTs are performed using Gaussian windows with the k-range of 3–17 Å^{-1} for the Se K-edge, 3–14 Å^{-1} for the Te L_1-edge and 3–16 Å^{-1} for the Fe K-edge EXAFS oscillations. The vertical dashed lines are guides to the eyes. Model fits to the FTs are also shown as solid lines (see text).

18132 | *Phys. Chem. Chem. Phys.,* 2015, **17**, 18131–18137

This journal is © the Owner Societies 2015

and Fe atoms. The main peak in the FTs of the Se K-edge EXAFS ($R \sim 2.3$ Å) contains information on the Se–Fe bondlength since Se atoms in the structure are tetrahedrally coordinated with four Fe atoms. The Fe–Se distance in the binary FeSe is expected to be ~ 2.4 Å. On the other hand, the main peak in the FTs of the Te L_1-edge EXAFS ($R \sim 2.5$ Å) is due to Te–Fe scatterings, providing information on this distance, known to be ~ 2.6 Å in the binary FeTe system. The peaks at longer distances in the FTs of two edges are due to distant shells mixed with the multiple scattering contributions. The contributions of Fe–Se (Se K-edge) and Fe–Te (Te L_1-edge) bondlengths in the FTs of two edges hardly show any change with Te-concentration, indicating that the Fe–Se distance in ternary FeSe$_{1-x}$Te$_x$ remains to be the same as in binary FeSe. Similarly, the Fe–Te distance in ternary FeSe$_{1-x}$Te$_x$ remains similar to the one in binary FeTe. Therefore, the Se and Te atoms in ternary FeSe$_{1-x}$Te$_x$ are sitting at different positions from the Fe atoms, with distinct Fe–Se and Fe–Te distances. This is a clear indication of the local structure of FeSe$_{1-x}$Te$_x$ being different from the known average crystallographic structure of FeSe$_{1-x}$Te$_x$. These indications are consistent with earlier local structure studies.[11,13,14] Similarly, the double peak structure in the FTs of the Fe K-edge EXAFS contains information on both Fe–Se/Te and Fe–Fe bondlengths since Fe atoms in the structure are tetrahedrally coordinated by four Se/Te atoms at a distance of ~ 2.4 Å, and four Fe atoms at ~ 2.7 Å. The main FT peak of the Fe K-edge EXAFS shows some apparent changes with changing Te concentration due to the evolving bondlengths.

To determine local structure parameters, the EXAFS oscillations measured on FeSe$_{1-x}$Te$_x$ at different edges were modeled by the EXAFS equation[22] based on the single-scattering approximation:

$$\chi(k) = \sum_i \frac{N_i S_0^2}{k R_i^2} f_i(k, R_i) e^{-\frac{2R_i}{\lambda}} e^{-2k^2 \sigma_i^2} \sin[2kR_i + \delta_i(k)]$$

where N_i is the number of neighbouring atoms at a distance R_i, δ_i is the phase shift, $f_i(k, R_i)$ is the backscattering amplitude, λ is the photoelectron mean free path, and σ_i^2 is the correlated Debye–Waller factor (DWF) measuring the mean square relative displacement (MSRD) of the photoabsorber–backscatter pairs. The S_0^2 is the so-called passive electron reduction factor, *i.e.*, the EXAFS amplitude reduction factor due to many-body effects related to the losses occurring during the photoelectron propagation in the material (excitations as plasmons, electron–hole pairs, *etc.*) and the intrinsic losses due to shake-up and shake off excitations created by the core–hole in the absorption process. In general, chemical transferability[22,26] is an appropriate procedure for the estimation of S_0^2 considering difficulties in quantifying the many-body effects.

The average structure measured by the diffraction on the FeSe$_{1-x}$Te$_x$ system[28–30] was used as the starting model for the least-squares fits of the EXAFS oscillations. The fact that Se and Te have nearest neighbour Fe atoms and the contributions of Se–Fe (in the Se K-edge EXAFS) and Te–Fe (in the Te L_1-edge

EXAFS) are well separated from higher shells and hence the EXAFS due to these have been analyzed using single shells. On the other hand, three shell model fits, involving the contributions of Fe–Se, Fe–Te and Fe–Fe were employed for the analysis of the Fe K-edge EXAFS. Furthermore, the Fe–Se and Fe–Te distances in the Fe K-edge EXAFS analysis were fixed to the one obtained from the Se K-edge and the Te L_1-edge EXAFS analysis. The EXCURVE 9.275 code (with calculated backscattering amplitudes and phase shift functions)[31] was used for the model fits. Only the radial distances R_i and the corresponding σ_i^2 were allowed to vary in the least-squares model fits, with the coordination number (N_i) fixed to the nominal values. The other two fit parameters (photoelectron energy zero E_0 and the scale factor given by the passive electron reduction factor S_0^2) were also fixed after fit trials on different scans. The number of independent data points, $N_{ind} \sim (2\Delta k \Delta R)/\pi$,[22] was about 16 (interval in k-space $\Delta k = 14$ Å^{-1} and interval in R-space $\Delta R = 1.8$ Å) and 13 ($\Delta k = 11$ Å^{-1} and $\Delta R = 1.8$ Å), respectively, for the Se K-edge EXAFS and Te L_1-edge EXAFS analyses with the number of fit parameters being two. The N_{ind} for the Fe K-edge EXAFS was about 18 ($\Delta k = 13$ Å^{-1} and $\Delta R = 2.2$ Å) for the six parameter fits. The uncertainties were determined by creating correlation maps[22,26,32] and analysing four different absorption scans for each sample. The model fits in the real space are shown as solid lines in Fig. 1.

Fig. 2 shows local Fe–Ch (Fe–Se and Fe–Te) bondlengths in FeSe$_{1-x}$Te$_x$ as a function of Te-substitution, determined by the Se K-edge and Te L_1-edge EXAFS model fits. The Fe–Fe distance, determined by the Fe K-edge EXAFS, is shown in Fig. 2(b). The Fe–Se and Fe–Te distances in ternary FeSe$_{1-x}$Te$_x$ are similar to the Fe–Se distance in the binary FeSe system (~ 2.4 Å) and the Fe–Te distance in the binary FeTe system (~ 2.6 Å). It is clear from these results that the Se and Te atoms in the ternary systems are displaced from the average crystallographic sites, *i.e.*, the nanoscale structure of ternary FeSe$_{1-x}$Te$_x$ is characterized by distinct Fe–Se and Fe–Te bonds. This is consistent with earlier EXAFS results in which Se K- and Fe K-edges were used,[11,13,14] revealing random-alloy like local structure of FeSe$_{1-x}$Te$_x$. Here, we have carried out the EXAFS measurements on several samples and, in addition to Se K and Fe K-edges, Te L_1-edge EXAFS has been used to extract direct information on the Fe–Te distance where the first peak in the FT magnitude contains only a single contribution without any mixing from the contribution from other distances (see Fig. 1 middle panel). Unlike the Fe–Se (Te) distances, the Fe–Fe distance, determined by the Fe K-edge EXAFS, is consistent with the average structure measured by diffraction experiments.[27–30]

As discussed earlier, the diverging local structure of ternary FeSe$_{1-x}$Te$_x$ from its average crystallographic structure is similar to the case of the random alloys of the type AB$_{1-x}$C$_x$ in which the local structure of the ternary, with non-equivalent bondlengths A–B and A–C, is known to diverge from the average crystallographic structure.[33–37] These local displacements in the random alloys reflect lower local symmetry of the crystal associated with the strain–relaxation arrangement of the atomic sites. The nearest-neighbour distances in ternary alloys
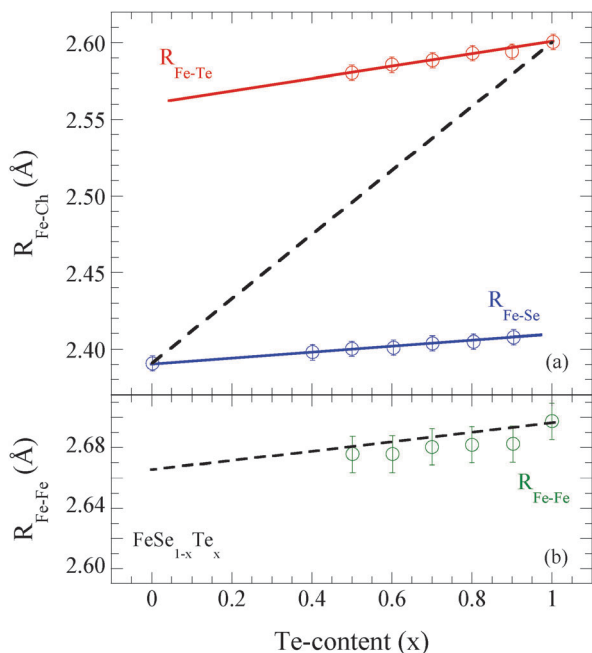
This journal is © the Owner Societies 2015

Phys. Chem. Chem. Phys., 2015, **17**, 18131–18137 | **18133**

Fig. 2 Fe–Se and Fe–Te distances determined by EXAFS and the average Fe–Ch distance (dashed line) as a function of Te concentration showing the characteristic Z-plot of the random alloys (upper). The dashed line is the average Fe–Ch distance, consistent with the diffraction measurements. The Fe–Fe distance is shown in (b) alongwith the one measured by diffraction (dashed line) as a function of Te concentration (lower). The error bars represent maximum uncertainty, determined using correlation maps between different parameters and by analyzing different EXAFS scans.
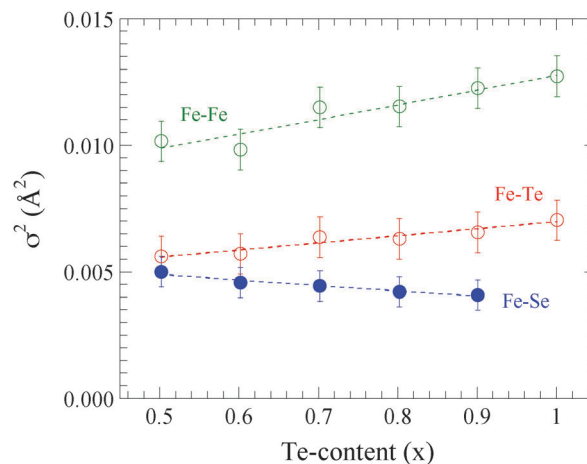

Fig. 3 Mean square relative displacements (σ^2) for Fe–Se, Fe–Te and Fe–Fe bondlengths are plotted as a function of Te-concentration in $FeSe_{1-x}Te_x$. For a consistent comparison the σ^2 determined from the Fe K-edge EXAFS alone are shown.

are characterized by the so-called Z-plot.[33–37] A similar Z-plot can be seen for ternary $FeSe_{1-x}Te_x$ in Fig. 2. It is clear that the local Fe–Se and Fe–Te bondlengths are closer to those in the binary end-members (FeSe and FeTe) than what one expects from the prediction of Vegard's law[16] (dashed line). It is worth underlining that for ordered alloys Vegard's law is expected to be satisfied, *i.e.*, a large probability of occupying the same site by different atoms (Se and Te), and hence a single bondlength (Fe–Ch). In the present work, using a unique approach based on the site selective experimental probe, it is shown that Vegard's law is not satisfied for $FeSe_{1-x}Te_x$, revealing nanoscale inhomogeneity.

The dimensionless relaxation parameter ε in the ternary random alloys $AB_{1-x}C_x$ is defined as the difference between $d_{AC}^{AB:C}$ and the (unperturbed) first nearest-neighbour distance of the host d_{AB}^0 relative to the difference in the first nearest-neighbour distances of the two binaries, *i.e.*, $\varepsilon = (d_{AC}^{AB:C} - d_{AB}^0)/(d_{AC}^0 - d_{AB}^0)$. In the Pauling limit,[16] in which the atomic radii are approximately conserved in different environments, the two bonds will be composition independent and equal to their ideal values d_{AB}^0 and d_{AC}^0, and therefore $\varepsilon = 1$ (full relaxation). On the other hand, in Vegard's limit[16] $\varepsilon = 0$ (no relaxation) in which the alloy is expected to have a single (average) chemical bond (*i.e.*, no bond alteration). Here, ε is ∼0.93–0.95, indicating large average bond relaxation, unlike a large part of pseudobinary semiconductor alloys in which the relaxation parameter ε is ∼0.8.[33–37]

Further information on the atomic disorder is accessed from σ_i^2 of different bond distances. Fig. 3 displays σ^2 of the Fe–Se, Fe–Te and Fe–Fe pairs as a function of Te-substitution for $FeSe_{1-x}Te_x$, containing information on the configurational (static and dynamic) disorder.[22] It is known that the absolute values of σ_i^2 are sensitive to the k-range used in the EXAFS analysis. Indeed, while σ_i^2 values of the Fe–Se bondlength measured by the Se K-edge and the Fe K-edge were found to be similar due to a similar k-range (3–17 Å^{-1} and 3–16 Å^{-1} respectively), σ_i^2 for the Fe–Te bondlength, measured by the Te L_1-edge and Fe K-edge, were quantitatively different due to different k-ranges (3–14 Å^{-1} and 3–16 Å^{-1} respectively) used (even though the Te concentration dependence remains similar). Therefore, for a consistent comparison we have shown σ^2 of three bondlengths obtained from the Fe K-edge. σ^2 of the Fe–Se bondlength is found to be slightly lower than σ^2 of the Fe–Te bondlength, likely to be due to the fact that Te is heavier than Se. In general, σ^2 shows small changes with Te-substitution; the one for the Fe–Se tending to decrease unlike the one for the Fe–Te showing a tendency to increase. σ^2 of the Fe–Fe bondlength is substantially larger than those for the other bondlengths and tends to increase with Te-concentration. Apparently σ^2 values for all three bondlengths are larger than those expected for these bondlengths considering Einstein like stretching of atomic pairs, likely to be due to larger configurational static disorder caused by the random alloying.[11,15]

Let us move to discuss the XANES spectra, providing information on the local structure as well as the valence electronic states[22,38] as a function of Te-concentration. We have analyzed the XANES spectra measured on $FeSe_{1-x}Te_x$ at three different absorption edges (at the Fe K-edge, Se K-edge and Te L_1-edge). The XANES spectra measured on $FeSe_{1-x}Te_x$ for selected Te-concentrations are shown in Fig. 4. The spectra are normalized with respect to the atomic absorption estimated by a linear fit far away from the absorption edges. Different XANES features in the Fe K-edge (left) are marked as P, A, B and C,
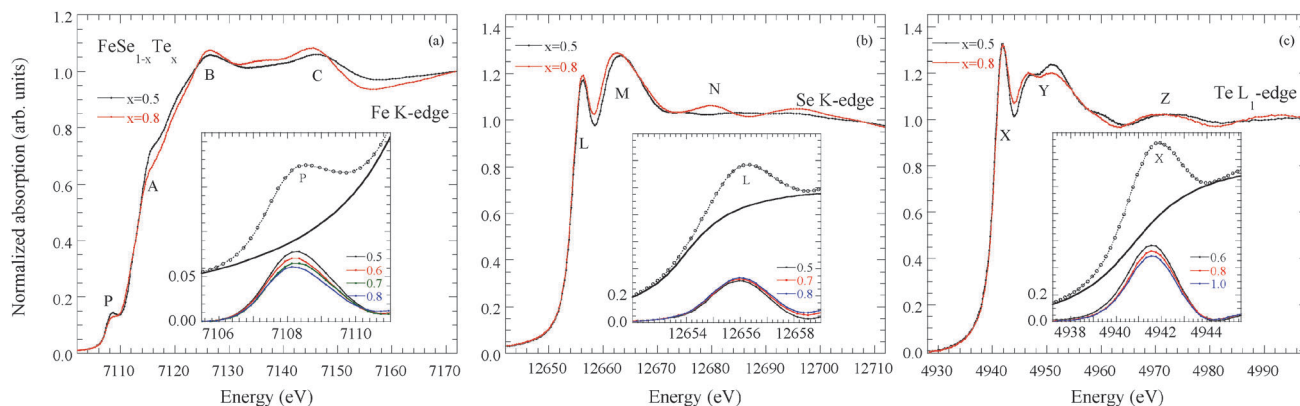
18134 | *Phys. Chem. Chem. Phys.*, 2015, **17**, 18131–18137

This journal is © the Owner Societies 2015

Fig. 4 Normalized XANES spectra of $FeSe_{1-x}Te_x$ measured at Fe K-edge (left), Se K-edge (middle) and Te L_1-edge (right). The features in the Fe K-edge XANES are denoted by P, A, B, C. Similarly, the Se K-edge and Te L_1-edge XANES features denoted respectively as L, M, N and X, Y, Z. The insets are zoom over the first transition features P, L and X alongwith the backgrounds determined by arctan functions. The back ground substracted peaks at several Te concentrations are also included in the inset.

while that in the Se K-edge (middle) and Te L_1-edge (right) are denoted by L, M, N and X, Y, Z, respectively. The Fe K-edge XANES spectra show an asymmetric pre-edge peak P due to the unoccupied Fe 3d mixed with the p states[39,40] and near edge features A, B and C due to the multiple scattering of the photoelectron excited from the Fe 1s core states. The pre-edge peak P exhibits a small change indicating the evolution of the unoccupied Fe 3d–p electronic states[39,40] with Te-concentration. Unlike the Fe K-edge XANES, there is a sharp peak feature L ($\sim 12\,655$ eV) in the Se K-edge XANES due to a direct 1s → 4p dipole allowed transition. Also a broad hump M (about 7 eV above the peak L) and a distant feature N can be seen, driven by the multiple scattering of the photoelectron with the nearest neighbours.[40] Here, peak L is a direct probe of the unoccupied Se 4p states which are affected by mixing with the Fe 3d states. Similarly, Te L_1-edge XANES spectra reveal a clear peak X due to a direct 2s → 5p dipole allowed transition, accompanied by a broad doublet Y and a distant feature Z due to multiple scattering of the photoelectron with the nearest neighbours. The multiple scattering features show a clear change due to changing local structure with Te concentration (see, *e.g.*, M in the Se K-edge and Y in the Te L_1-edge, revealing overall energy shifts towards lower energy due to longer bondlengths at higher Te-concentration).

In order to study the evolution of the unoccupied electronic states as a function of Te-concentration, measured by different XANES transitions, we have focussed only on the first transition peak features (P, L and X) in the XANES spectra measured at different edges. We have shown the zoomed absorption spectra in the region of features P, L and X containing the background (estimated by arctan functions) as insets of different panels in Fig. 4. Background-subtracted XANES spectra for different Te-concentrations are also included in the insets, revealing a clear evolution of the features P, L and X. The integrated intensities of peaks P, L and X are shown as a function of Te-concentration in Fig. 5.

Let us attempt to understand the XANES results revealing a clear change in the site-selective unoccupied electronic states
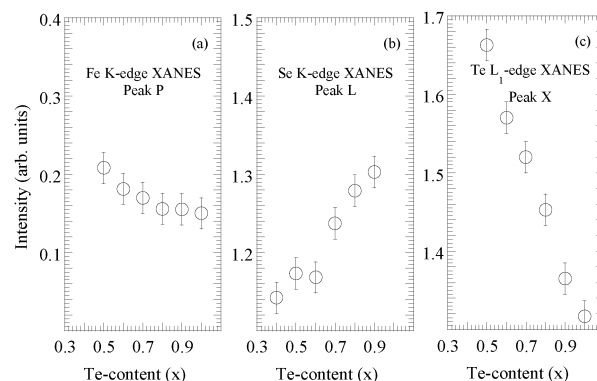

Fig. 5 Te dependence of peak P (left), L (middle) and X (right) intensities in $FeSe_{1-x}Te_x$, showing a clear change in the electronic structure of the unoccupied states. The peak P shows a small decrease while the peak L shows a substantial increase with Te-concentration. Peak X reveals the largest change with Te-concentration, showing a clear decrease in the unoccupied Te 5p electronic states. The error bars represent maximum uncertainties estimated by analysis of four different XANES spectra.

with Te-substitution in $FeSe_{1-x}Te_x$. The change in the pre-peak P intensity (Fig. 5a) reflects a decrease in unoccupied Fe 3d states with increasing Te-substitution. This is consistent with earlier experimental and theoretical reports,[39–41] and likely to be due to decreased overall admixing of Se 4p/Te 5p states with Fe 3d orbitals. In this case, an increase in the atomic-like Se 4p/Te 5p unoccupied states is expected with increasing Te-content. This can be checked independently from Se K and Te L_1-edges. Indeed, the Se 4p unoccupied states, determined by the Se K-edge XANES peak L intensity (Fig. 5b), show a gradual increase with Te-concentration. This is a further indication that the Fe 3d and Se 4p are substantially admixed as the Fe–Se bond is highly covalent. This mixing (between d_{xz}/d_{yz} and Se 4p) is expected to decrease due to a small increase in the Fe–Se bondlength (Fig. 2). The fact that the Fe–Se distance does not show an appreciable change with Te, while the Se 4p unoccupied states reveal a clear increase, is a mere indication of orbital selective admixing of the Se 4p

states since the d_{xz}/d_{yz} and d_{xy} orbitals exchange their energy positions going from FeSe to FeTe.[42]

On the other hand, the Te 5p unoccupied states suffer a clear decrease with Te-substitution (Fig. 5c). Although, Te 5p states have smaller hybridization with Fe 3d states, the higher polarizability of Te seems to have an important role in the electronic states and bonding properties. Indeed, charge transfer energy decreases with the increasing Te-content in $FeSe_{1-x}Te_x$.[39,43] Therefore, the Te 5p states seem to get more delocalized with increasing Te, and hence a decrease in unoccupied states can be expected.

4 Conclusions

In summary, we have studied the local and electronic structures of the unoccupied valence states in $FeSe_{1-x}Te_x$ as a function of Te-concentration by Fe K-, Se K- and Te L_1-edges EXAFS and XANES measurements. The EXAFS results show that the nano-scale structure of the ternary $FeSe_{1-x}Te_x$ chalcogenides diverges from the average crystallographic structure, and characterized by the coexistence of a random distribution of distinct Fe–Se and Fe–Te bondlengths. It is found that Vegard's limit is not satisfied and Pauling's limit is more plausible for describing the substitution in the $FeSe_{1-x}Te_x$ system in which highly relaxed distribution gives rise to the random-alloy like nano-scale structure. The XANES spectra reveal that Fe 3d–Se 4p/Te 5p hybridization decreases with increasing Te-substitution. The unoccupied Se 4p states show an increase with a concomitant decrease in the Te 5p states with the increasing Te-content. As the $FeSe_{1-x}Te_x$ is a multiband system, the observed nanoscale inhomogeneity in these materials should have direct implications for their electronic properties.[42] Indeed, electronic structure measurements and theoretical calculations are found to be consistent with the random atomic disorder in the ternary $FeSe_{1-x}Te_x$ system with direct implications for the electronic and magnetic properties of these materials.

Acknowledgements

References

1 F. C. Hsu, J.-Y. Luo, K.-W. Yeh, T.-K. Chen, T.-W. Huang, P. M. Wu, Y.-C. Lee, Y.-L. Huang, Y.-Y. Chu, D.-C. Yan and M.-K. Wu, *Proc. Natl. Acad. Sci. U. S. A.*, 2008, **105**, 14262.

2 A. Subedi, L. Zhang, D. J. Singh and M. H. Du, *Phys. Rev. B: Condens. Matter Mater. Phys.*, 2008, **78**, 134514.

3 T. Miyake, K. Nakamura, R. Arita and M. Imada, *J. Phys. Soc. Jpn.*, 2010, **79**, 044705.

4 K. Ishida, Y. Nakai and H. Hosono, *J. Phys. Soc. Jpn.*, 2009, **78**, 062001.

5 D. C. Johnston, *Adv. Phys.*, 2010, **59**, 803.

6 Y. Mizuguchi and Y. Takano, *J. Phys. Soc. Jpn.*, 2010, **79**, 102001.

7 K.-W. Yeh, T.-W. Huang, Y.-L. Huang, T.-K. Chen, F.-C. Hsu, P. M. Wu, Y.-C. Lee, Y.-Y. Chu, C.-L. Chen, J.-Y. Luo, D.-C. Yan and M.-K. Wu, *EPL*, 2008, **84**, 37002.

8 Y. Mizuguchi, F. Tomioka, S. Tsuda, T. Yamaguchi and Y. Takano, *J. Phys. Soc. Jpn.*, 2009, **78**, 074712.

9 Y. Mizuguchi, F. Tomioka, S. Tsuda, T. Yamaguchi and Y. Takano, *Appl. Phys. Lett.*, 2008, **93**, 152505.

10 S. Medvedev, T. M. McQueen, I. A. Troyan, T. Palasyuk, M. I. Eremets, R. J. Cava, S. Naghavi, F. Casper, V. Ksenofontov, G. Wortmann and C. Felser, *Nat. Mater.*, 2009, **8**, 630.

11 B. Joseph, A. Iadecola, A. Puri, L. Simonelli, Y. Mizuguchi, Y. Takano and N. L. Saini, *Phys. Rev. B: Condens. Matter Mater. Phys.*, 2010, **82**, 020502(R).

12 D. Louca, K. Horigane, A. Llobet, P. Tong and K. Yamada, *Phys. Rev. B: Condens. Matter Mater. Phys.*, 2010, **81**, 134524.

13 A. Iadecola, B. Joseph, L. Simonelli, Y. Mizuguchi, Y. Takano and N. L. Saini, *EPL*, 2010, **90**, 67008.

14 A. Iadecola, B. Joseph, A. Puri, L. Simonelli, Y. Mizuguchi, D. Testemale, O. Proux, J. L. Hazemann, Y. Takano and N. L. Saini, *J. Phys.: Condens. Matter*, 2011, **23**, 425701.

15 N. L. Saini, *Sci. Technol. Adv. Mater.*, 2013, **14**, 014401.

16 see, *e.g.*, *Ternary and multinary compounds*, ed. S. K. Deb and A. Zunger, Materials Research Society, Pittsburg, 1987.

17 H. Hu, J.-M. Zuo, J. Wen, Z. Xu, Z. Lin, Q. Li, G. Gu, W. K. Park and L. H. Greene, *New J. Phys.*, 2011, **13**, 053031.

18 W. Z. Lin, Q. Li, B. C. Sales, S. Jesse, A. S. Sefat, S. V. Kalinin and M. H. Pan, *ACS Nano*, 2013, **7**, 2634.

19 U. R. Singh, S. C. White, S. Schmaus, V. Tsurkan, A. Loidl, J. Deisenhofer and P. Wahl, *Phys. Rev. B: Condens. Matter Mater. Phys.*, 2013, **88**, 155124.

20 T. Kato, Y. Mizuguchi, H. Nakamura, T. Machida, H. Sakata and Y. Takano, *Phys. Rev. B: Condens. Matter Mater. Phys.*, 2009, **80**, 180507(R).

21 X. He, G. Li, J. Zhang, A. B. Karki, R. Jin, B. C. Sales, A. S. Sefat, M. A. McGuire, D. Mandrus and E. W. Plummer, *Phys. Rev. B: Condens. Matter Mater. Phys.*, 2011, **83**, 220502(R).

22 D. C. Koningsberger and R. Prins, *X-Ray Absorption: Principles, Applications, Techniques of EXAFS, SEXAFS and XANES*, Wiley, New York, 1988.

23 M. Y. Hacisalihoglu, 2011, Dissertation in Physics, Trabzon Karadeniz Technical University; M. Y. Hacisalihoglu and E. Yanmaz, 2011, 5th National Superconductivity Symposium, Izmir, TURKEY, unpublished.

24 H. Okamoto, *J. Phase Equilib.*, 1991, **12**, 383.

25 H. Okamoto and L. E. Tanner, *Bull. Alloy Phase Diagrams*, 1990, **11**, 371.

26 G. G. Li, F. Bridges and C. H. Booth, *Phys. Rev. B: Condens. Matter Mater. Phys.*, 1995, **52**, 6332.

27 K. Horigane, H. Hiraka and K. Ohoyama, *J. Phys. Soc. Jpn.*, 2009, **78**, 074718.

28 S. Li, C. de la Cruz, Q. Huang, Y. Chen, J. W. Lynn, J. Hu, Y.-L. Huang, F.-C. Hsu, K.-W. Yeh, M.-K. Wu and P. Dai, *Phys. Rev. B: Condens. Matter Mater. Phys.*, 2009, **79**, 054503.

29 W. Bao, Y. Qiu, Q. Huang, M. A. Green, P. Zajdel, M. R. Fitzsimmons, M. Zhernenkov, S. Chang, M. Fang, B. Qian, E. K. Vehstedt, J. Yang, H. M. Pham, L. Spinu and Z. Q. Mao, *Phys. Rev. Lett.*, 2009, **102**, 247001.

30 B. C. Sales, A. S. Sefat, M. A. McGuire, R. Y. Jin, D. Mandrus and Y. Mozharivsky, *Phys. Rev. B: Condens. Matter Mater. Phys.*, 2009, **79**, 094521.

31 S. J. Gurman, *J. Synchrotron Radiat.*, 1995, **2**, 56.

32 R. W. Joyner, K. J. Martin and P. Meehan, *J. Phys. C: Solid State Phys.*, 1987, **20**, 4005.

33 J. C. Mikkelsen Jr. and J. B. Boyce, *Phys. Rev. Lett.*, 1982, **49**, 1412.

34 A. Balzarotti, M. Czyzyk, A. Kisiel, N. Motta, M. Podgrny and M. Zimnal-Starnawska, *Phys. Rev. B: Condens. Matter Mater. Phys.*, 1984, **30**, 2295.

35 Q. T. Islam and B. A. Bunker, *Phys. Rev. Lett.*, 1987, **59**, 2701.

36 N. Happo, H. Sato, T. Mihara, K. Mimura, S. Hosokawa, Y. Ueda and M. Taniguchi, *J. Phys.: Condens. Matter*, 1996, **8**, 4315.

37 P. F. Peterson, T. H. Proffen, I.-K. Jeong, S. J. L. Billinge, K.-S. Choi, M. G. Kanatzidis and P. G. Radaelli, *Phys. Rev. B: Condens. Matter Mater. Phys.*, 2001, **63**, 165211.

38 J. Garcia, A. Bianconi, M. Benfatto and C. Natoli, *J. Phys., Colloq.*, 1986, **47**(C8), C8-49–C8-54.

39 L. Simonelli, N. L. Saini, Y. Mizuguchi, Y. Takano, T. Mizokawa, G. Baldi and G. Monaco, *J. Phys.: Condens. Matter*, 2012, **24**, 415501.

40 B. Joseph, A. Iadecola, L. Simonelli, Y. Mizuguchi, Y. Takano, T. Mizokawa and N. L. Saini, *J. Phys.: Condens. Matter*, 2010, **22**, 485702.

41 A. Vega-Flick, J. Mustre de Leon and N. L. Saini, *J. Phys. Chem. Solids*, 2015, **84**, 80.

42 T. Sudayama, D. Ohtsuki, Y. Wakisaka, T. Mizokawa, N. L. Saini, M. Arita, H. Namatame, M. Taniguchi, T. Noji and Y. Koike, *J. Phys. Soc. Jpn.*, 2013, **82**, 053705.

43 N. L. Saini, Y. Wakisaka, B. Joseph, A. Iadecola, S. Dalela, P. Srivastava, E. Magnano, M. Malvestuto, Y. Mizuguchi, Y. Takano, T. Mizokawa and K. B. Garg, *Phys. Rev. B: Condens. Matter Mater. Phys.*, 2011, **83**, 052502.

This journal is © the Owner Societies 2015

Phys. Chem. Chem. Phys., 2015, **17**, 18131–18137 | **18137**